ROYAL SOCIETY
OF CHEMISTRY

PAPER

Grain boundary dominated charge transport in Mg$_3$Sb$_2$-based compounds[†]

Jimmy Jiahong Kuo,[a‡] Stephen Dongmin Kang,[ab‡] Kazuki Imasato,[a] Hiromasa Tamaki,[c] Saneyuki Ohno,[abd] Tsutomu Kanno,[c] and G. Jeffrey Snyder[*a]

Thermally activated mobility near room temperature is a signature of detrimental scattering that limits the efficiency and figure-of-merit zT in thermoelectric semiconductors. This effect has been observed dramatically in Mg$_3$Sb$_2$-based compounds, but also to a lesser extent in other thermoelectric compounds. Processing samples differently or adding impurities such that this effect is less noticeable produces materials with a higher zT. Experiments suggest that the behavior is related to grain boundaries, but impurity scattering has also been proposed. However, conventional models using Matthissen's rule are not able to explain the dramatic change in the temperature dependency of conductivity or drift mobility which is observed in Mg$_3$Sb$_2$-based compounds. We find that it is essential to consider the grain boundary region as an effectively separate phase rather than a scattering center, taking into account the weaker screening in semiconductors compared with classical metals. By modeling a grain boundary phase with a band offset, we successfully reproduce the experimentally observed conductivity versus temperature and thermopower versus conductivity relations, which indicate an improved description of transport. The model shows good agreement with measured grain size dependencies of conductivity, opening up avenues for quantitatively engineering materials with similar behavior. Model estimates predict room for $> 60\%$ improvement in the room temperature zT of Mg$_{3.2}$Sb$_{1.5}$Bi$_{0.49}$Te$_{0.01}$ if the grain boundary resistance could be eliminated.

Broader Context

To devise strategies for improving the thermeoelctric performance of materials, it is essential to understand the charge transport mechanism. When inferring the dominant mechanism, the temperature dependency of conductivity or mobility is one of the signatures first considered. A particular case of recent interest is when mobility increases with temperature in degenerate semiconductors, which is often attributed to the kind of scattering events that decreases with temperature such as ionized impurity scattering. However, the inadequacy of such descriptions becomes apparent when trying to consistently explain various experimental observations like the enhanced mobilities in larger grain samples and sharp crossovers to metal-like decreasing mobilities with temperature. The underlying cause of such complications is largely associated with the conventional paradigm that interprets or models all of the charge carrier scattering as homogeneous events. The inhomogeneous nature of materials, such as that caused by grain boundaries, must be taken into account to rethink engineering strategies and further improve thermoelectric materials.

Thermoelectric materials provide a clean and reliable way of generating electricity from waste heat.[1] The maximum conversion efficiency of a thermoelectric material is determined by the dimensionless figure of merit, $zT = S^2 \sigma T / \kappa$, where S is the Seebeck coefficient, σ is the electrical conductivity, T is the absolute temperature, and κ is the thermal conductivity. For high power thermoelectric generation, it is desired to have a large temperature difference and also a zT that is high throughout the given temperature range. Therefore, the zT near the cold side temperature, usually around room temperature, is as important as the peak zT at high temperature.[2]

In some promising high temperature thermoelectric materials such as Mg$_3$Sb$_2$,[3] SnSe,[4] KAlSb$_4$,[5] Sr$_3$GaSb$_3$,[6] NbFeSb,[7] Ca$_5$Al$_2$Sb$_6$,[8] and Ca$_3$AlSb$_3$,[9] it is not uncommon to find thermally activated behavior in the low temperature conductivity despite being a degenerate semiconductor that is expected to behave like a metal. Associated with this behavior is a relatively low conductivity (from a low mobility) that compromises the low temperature zT.

Recently, n-type Mg$_3$Sb$_2$-based compounds were discovered[3]

with a high peak zT causing great interest in the related compounds.[10–12] However, at room temperature the compound tends to show thermally activated conductivity, the degree of which depending significantly on sample variation and preparation. In previous reports,[11,13–15] such behavior was attributed to ionized-impurity scattering (IIS) of the charge carriers which then show the more typical acoustic-phonon scattering (APS) behavior above 500 K; the temperature dependency of mobility or conductivity resembled that of IIS ($T^{3/2}$) and APS ($T^{-3/2}$) at low and high temperatures, respectively.

We find here that the transport behavior of Mg_3Sb_2-based compounds is more complex than what a simple temperature-dependency analysis might suggest, involving resistive grain boundaries that make the material behave effectively like an inhomogeneous material. Building upon experimental evidence and analysis on the thermopower-conductivity relation, we show that IIS does not provide an adequate description for Mg_3Sb_2-based compounds. We instead propose a two-phase model to describe grain-boundary dominated material systems.

1 Motivation for an inhomogeneous model

Although the previously suggested homogeneous IIS scattering model can qualitatively explain a mobility and conductivity that rise with temperature, it is unable to provide a consistent picture for electronic transport in Mg_3Sb_2-based compounds. Quantitatively, it can be shown that such a dramatic change in the conductivity or drift mobility at 500 K cannot be described by mixing APS and IIS scattering events with the Matthiessen's rule (see ESI† for analytical proof).

This inadequacy of the IIS model can also be seen by investigating the thermopower ($|S|$) − conductivity (σ) relation ($\log|S| - \log\sigma$) which reflects the energy dependency[16] of the carrier scattering time. Measurements from $Mg_{3+x}Sb_{1.5}Bi_{0.5-y}Te_y$[17] analyzed in Fig.1 show that the $\log|S| - \log\sigma$ relation resembles that of APS rather than IIS.

Experimental evidence suggests that the description for transport in Mg_3Sb_2-based compounds should take into account grain boundary effects; it has been shown that the low temperature thermal activation behavior could be mitigated by increasing the grain size (*i.e.* decreasing the grain boundary density).[17]

Conventional grain boundary transport models for metals typically treat their contribution to resistance using Matthiessen's rule on the carrier scattering rate ($\tau^{-1} = \sum \tau_i^{-1}$; independent scattering assumption), which is designed for spatially homogeneous systems. The assumption for using this approach for grain boundaries is that the grain boundary region is physically small enough that the material could be approximated as a homogeneous system, just as point defects or impurities are modeled. This approach has been used to model metals,[18,19] but sometimes also for doped semiconductors such as SiGe.[20]

However, when charge screening is not as effective as in metals, the grain boundary could have a much stronger influence over extended lengths because the space-charge region induced by the grain boundary (in which carriers are depleted) becomes significantly extended to a thickness much greater than the grain

boundary itself.[21,22] For example, in Mg_3Sb_2, we estimate the depletion region due to a grain boundary to be around 10 nm based on a space-charge model,[21] which is comparable or even larger than the electron mean free path λ (*e.g.* a mobiltiy of 50 cm^2/V·s, Fermi velocity $\approx 10^6$ m/s, $m^* \approx 0.3m_e$ would yield $\lambda \approx 8$ nm). The formation of such a space-charge region is a generic phenomenon because grain boundaries generally induce electronic structure changes that lead to some charge transfer.[21]

An associated issue for describing grain boundaries with a homogeneous model using Matthiessen's rule on the carrier scattering rate is that it assumes an identical carrier concentration across the grain boundary region, which is an assumption that easily breaks down for extended grain boundary regions that have charge depletion. Use of Matthiessen's rule on mobility ($\mu^{-1} = \sum \mu_i^{-1}$) to describe grain boundaries[7,23] involve additional issues of failing to take into account the energy dependency of different scattering mechanisms.

Overall, we find that an explicit grain boundary transport model is needed to describe the inhomogeneous nature of the grain boundary region. This conclusion motivates us to construct a two-phase model where the grain-boundary induced space-charge region is treated as a separate phase connected with the grains of the material.
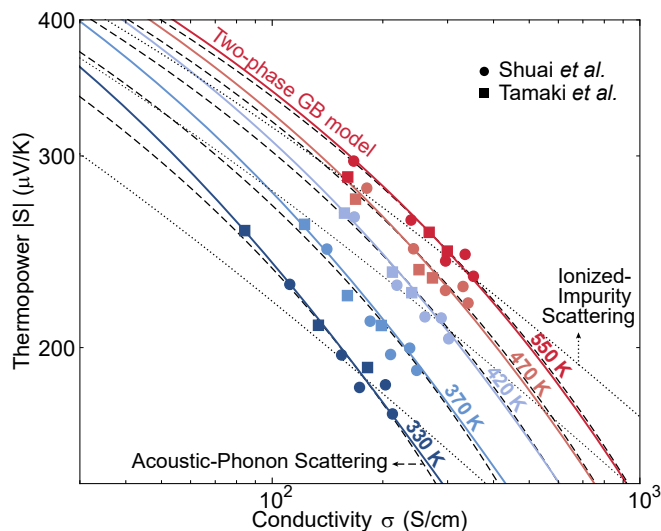

Fig. 1 A $\log|S|$-$\log\sigma$ plot to examine the energy dependency of transport in $Mg_{3+x}Sb_{1.5}Bi_{0.5-y}Te_y$. The data points are literature data from samples with similar properties but with different doping levels (*i.e.* varied Te content): circles from Ref.[11] and squares from Ref.[3]. The solid lines represent our two-phase model using the parameters listed in Table.1. The dashed and dotted lines show the curve shapes predicted by acoustic-phonon scattering and ionized-impurity scattering, respectively. The Seebeck coefficient above 600 K is significantly affected by bipolar[24] contributions and is thus not considered in this plot.

2 The Model

2.1 Band shifting near grain boundaries

The influence of grain boundaries on charge transport is generally understood in terms of a potential barrier produced as a result of charge transfer between the grain boundary and the grain.[21,22,25,26] The electronic structure at the grain boundary is

different from the grain because of lattice mismatch, defects, and impurities. This difference generally induces some charge transfer to maintain an equilibrated Fermi-level across the material, which results in space-charge regions near the grain boundary. When the resulting structure is such that a potential barrier is developed as illustrated in Fig.2, electric conductivity across the boundary could be significantly reduced.
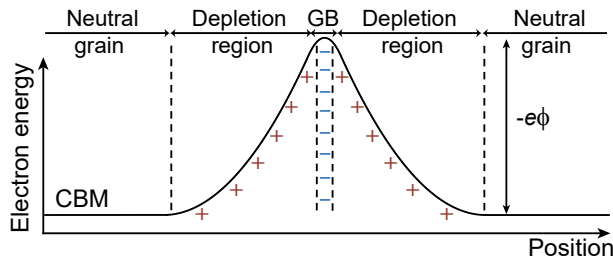

Fig. 2 Electron energy diagram of an n-type semiconductor with a potential barrier across the grain boundary. The majority carriers (*i.e.* electrons) are transferred from the grain to the grain boundary, resulting in a negatively-charged grain boundary (GB) and positively-charged depletion regions. CBM is the conduction band minimum and ϕ is the potential barrier height. Note that the grain boundary is drawn with a finite width for illustration.

2.2 A two-phase description with a band offset

In semiconductors, the depletion region is generally larger than in metals due to weaker screening, often being comparable to or larger than the electron mean free path at high temperatures. In such cases, the depletion region is better treated as a secondary phase with an energy-shifted band rather than a scattering center.

As a first-order approximation, we replace the spatial variation of the barrier potential with an effective band offset ΔE that is constant across the depletion region. The secondary phase describing the depletion region is thereby represented with a band structure identical to that of the neutral grain but with an effective band offset (Fig.3a). This approach allows the model to take into account the impact of the potential barrier with a minimal number of model parameters.

In general, the band offset ΔE depends not only on the microscopic details of the grain boundary, but also on the Fermi-level in the neutral grain because it determines how much charge must be transfered for equilibrium. [21] In other words, ΔE will generally be dependent on the doping level of the material. We empirically find a linear form (see ESI[†]):

$$\Delta E = \Delta E_0 + a \cdot E_{\mathrm{F,G}}, \qquad (1)$$

where ΔE is the offset in the charge-depleted phase with respect to the neutral grain phase. $E_{\mathrm{F,G}}$ is the Fermi-level in the neutral grain measured from the band edge (positive for increasing free carrier energy) and ΔE_0 is a reference band offset when $E_{\mathrm{F,G}} = 0$. The coefficient a is a fitting parameter to be determined empirically. This form of the band offset is within the feasible range of the space-charge model. [21]

Carrier transport through each phase is calculated using typical band transport equations. [16,27] Conductivity:

$$\sigma_i = \sigma_{E_0}(T) \cdot sF_{s-1}(\eta_i), \qquad (2)$$

the Seebeck coefficient:

$$S_i = \frac{k_{\mathrm{B}}}{e} \left[\frac{(s+1)F_s(\eta_i)}{sF_{s-1}(\eta_i)} - \eta_i \right], \qquad (3)$$

and the Lorenz number:

$$L_i = \left(\frac{k_{\mathrm{B}}}{e} \right)^2 \frac{s(s+2)F_{s-1}(\eta_i)F_{s+1}(\eta_i) - (s+1)^2 F_s^2(\eta_i)}{s^2 F_{s-1}^2(\eta_i)}. \qquad (4)$$

Here the subscript i denotes the phase, η is the reduced Fermi-level $E_{\mathrm{F}}/k_{\mathrm{B}}T$, F_j is the Fermi-Dirac integral $F_j(\eta) = \int_0^\infty \frac{\varepsilon^j d\varepsilon}{1+\exp(\varepsilon-\eta)}$, s is a parameter for the conduction mechanism, and σ_{E_0} is a transport coefficient that determines the magnitude of conductivity.

For the neutral grain phase, we use the acoustic-phonon scattering model ($s = 1$; $\sigma_{E_0} \propto T^0$); for the charge-depleted phase, we use an ionized-impurity scattering model ($s = 3$; $\sigma_{E_0} \propto T^3$) considering the presence of space-charges. The grain boundary interface itself is not explicitly assigned a phase, and its influence on the carrier mobility (*e.g.* charge trapping [28,29]) is effectively captured with σ_{E_0} of the charge-depleted phase. We simply refer to the two model phases as the "grain phase" and the "grain boundary phase."
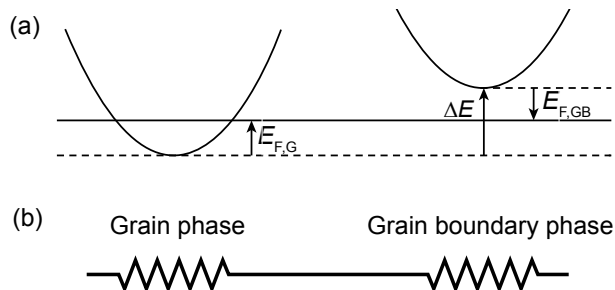

Fig. 3 (a) Energy band diagrams of the neutral grain phase and grain boundary phase. The potential barrier across the grain boundary (Fig.2) is taken into account with an offset ΔE between the two bands. The band offset relates the reference points of the Fermi-levels: $E_{\mathrm{F,GB}} = E_{\mathrm{F,G}} - \Delta E$ **(b)** The series circuit limit of the two-phase description.

2.3 The series circuit limit

A simplified model configuration where the grain phase and the grain boundary phase are connected in a series circuit (Fig.3b) is found to be sufficient in describing the essential features in conductivity and the Seebeck coefficient. We note that the series circuit configuration is one of the limiting cases of three dimensional two-phase models such as effective medium theory, and that the grain and thin boundary structure in those models is not far from the series circuit limit for conductivity or the Seebeck coefficient when there is a big difference between the grain and grain boundary phase conductivities. [30–32]

In the series circuit configuration, overall electrical conductivity

σ is calculated by:

$$\sigma^{-1} = (1 - t_{GB})\sigma_G^{-1} + t_{GB}\sigma_{GB}^{-1}, \qquad (5)$$

where the subscripts G and GB refer to the grain and grain boundary phase, respectively. t_{GB} is the size fraction of the grain boundary phase. Thermal conductivity is calculated identically by replacing σ_i's with thermal conductivities.

The Seebeck coefficient is calculated by:

$$S = \frac{S_G \frac{1-t_{GB}}{\kappa_G} + S_{GB} \frac{t_{GB}}{\kappa_{GB}}}{\frac{1-t_{GB}}{\kappa_G} + \frac{t_{GB}}{\kappa_{GB}}}, \qquad (6)$$

where κ is thermal conductivity. Since t_{GB} is very small and S_i's and κ_i's are similar in orders of magnitude between the two phases, Eq.6 reduces to:

$$S \approx S_G. \qquad (7)$$

It is seen that the thermopower is essentially unchanged due to the influence of a thin grain boundary whereas the conductivity could significantly change depending on the σ_G/σ_{GB} ratio. This feature of unchanging thermopower is indeed one of the experimental observations for grain boundary dominated materials in general, as exemplified in SiGe,[20] Mg$_2$Si,[23] CoSb$_3$,[33] and Ca$_3$AlSb$_3$.[9] By contrast, a Matthiessen's rule approach would typically predict a change in the Seebeck coefficient, which can be seen from Eq.3 where the Seebeck coefficient is dependent on the s parameter that reflects the energy dependency of scattering time.

Table 1 Model parameters for Mg$_{3+x}$Sb$_{1.5}$Bi$_{0.5-y}$Te$_y$.

Grain phase (G)	σ_{E_0}	$=$	900 S/cm
Grain boundary phase (GB)	σ_{E_0}	$=$	0.2 S/cm at 300 K
	t_{GB}	$=$	0.001
Band offset	ΔE_0	$=$	60 meV
	a	$=$	0.3

3 Results and discussion

3.1 Energy and temperature dependency of transport

The energy dependency of charge transport described by our model can be compared to experimental measurements by examining the $\log|S| - \log\sigma$ relation, as shown in Fig.1. The best fit of our model is in good agreement with the literature values across the temperature range. It is also seen that the shape of the model curve is very similar to that predicted by the typical APS model except in the high thermopower range, whereas the IIS model – suggested as the transport mechanism in earlier reports – predicts a curve that is distinctly different than either the data or our model.

Both the thermally activated conductivity and the transition to a metal-like slope in conductivity around 500 K are also well captured with our model, as can be seen in Fig.4.

In our model, the thermal activation behavior originates from the band offset between the grain and grain boundary phases. With increasing temperature, the effect of this band offset diminishes because charge carriers have more energy to overcome the barrier. As a result, above a certain crossover temperature the
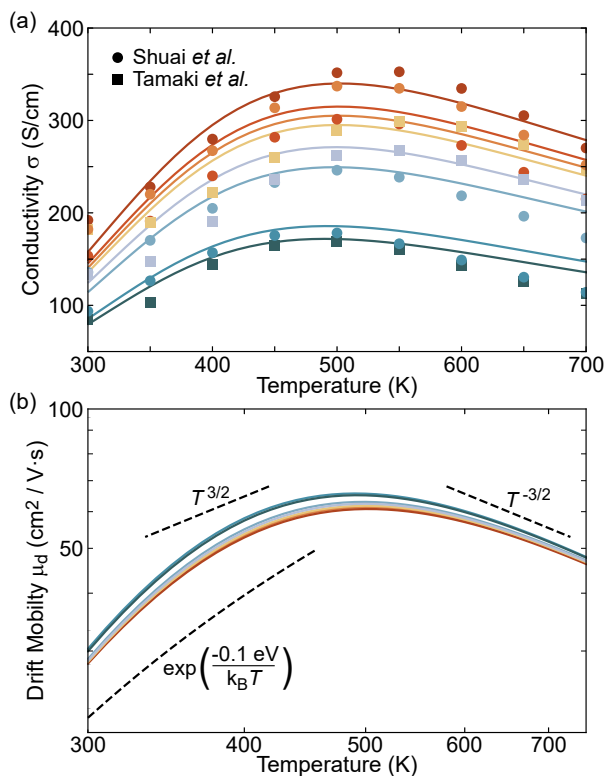

Fig. 4 (a) Conductivity change with respect to temperature observed in Mg$_{3+x}$Sb$_{1.5}$Bi$_{0.5-y}$Te$_y$. Below 500 K the conductivity increases with temperature, whereas at higher temperatures the trend is reversed. Data points are from the samples shown in Fig.1. The solid lines are from our model using the identical parameters as for Fig.1. The band offset function was fixed for the all samples (using Eq.1), rather than finding the best for each sample. Small discrepancies between the model and data could be attributed to sample variations having some deviations from the universal offset function. **(b)** Effective drift mobility with respect to temperature on a log-log plot. The curves were calculated from the model curves in (a) using carrier concentration-thermopower relations reported in the literature.[24] The high temperature mobility resembles the signature of acoustic-phonon scattering ($T^{-3/2}$). The low temperature dependency could apparently resemble either an IIS ($T^{3/2}$) or exponential dependency (or even a variable-range hopping type dependency[34]) if examined over a small temperature range.

transport behavior reverts to that of a typical metal or degenerate semiconductor.

The most critical model element required for reproducing the experimentally observed crossover in $d\log\sigma/d\log T$ is the presence of a band offset between the two phases, but not the IIS description ($s = 3$; $\sigma_{E_0} \propto T^3$) of the grain boundary phase. It is possible to produce equally satisfactory fits using an APS description ($s = 1$; $\sigma_{E_0} \propto T^0$) for the grain boundary phase. We use IIS for the charge-depleted phase only because it results in a more reasonable prediction of the band offset values and it is physically feasible that the scattering behavior in a space-charge region appear similar to IIS rather than APS.

3.2 Grain size dependency

Experimentally it has been shown that the thermally activated behavior of conduction could be tuned to some degree by changing

the grain size of the polycrystalline material. Our model successfully reproduces this grain size dependency by changing only the parameter related to grain size (t_{GB}), as shown in Fig.5a. The measured grain size increase is consistent with the of factor of six increase in the fitting parameter t_{GB}.
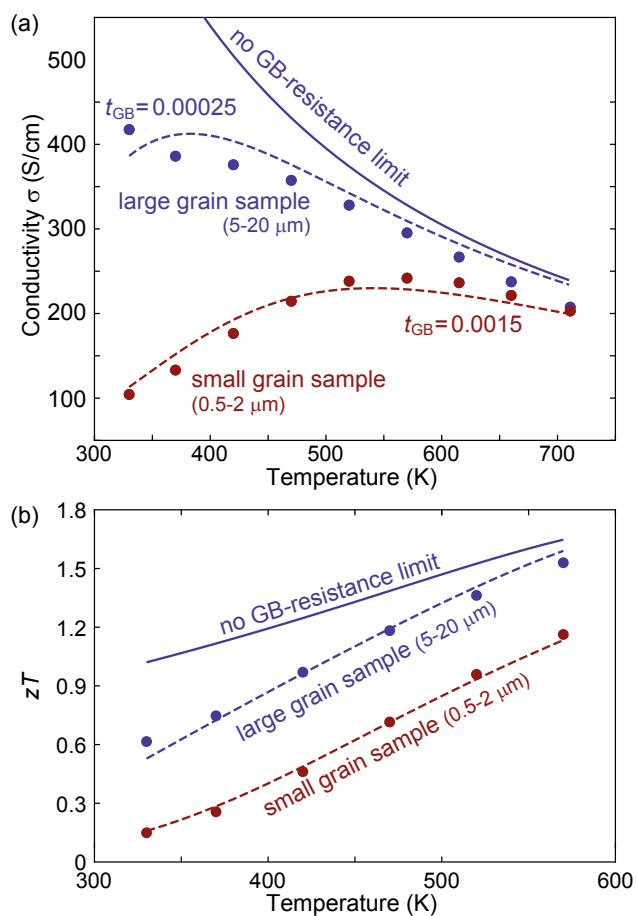

Fig. 5 (a) Thermally activated conduction behavior diminishing with increased grain size in $Mg_{3.2}Sb_{1.5}Bi_{0.49}Te_{0.01}$. The large grain sample (blue circles; 5-20 μm) shows higher conductivity than the small grain sample (red circles; 0.5-2 μm), and both samples are well described by the model (dashed lines) using parameters all identical but for t_{GB}. The limit of $t_{GB} = 0$ (solid line) is shown for comparison. **(b)** Upper limit of the figure-of-merit zT when the grain boundary phase resistance is zero (solid line), as estimated from our model. Model zT is calculated only in the range where bipolar contribution is negligible. Lattice thermal conductivity was extracted from experimental measurements by using our model to subtract the electronic thermal conductivity in both the grain and grain boundary phases and finding a self-consistent value. E_F was optimized at 330 K for the upper limit calculation. Data points are from Ref.[17].

3.3 Experimental strategies for material improvement

Based on our model understanding, it is possible to devise potential experimental strategies that could help to mitigate the mobility reduction caused by grain boundaries. Our analysis points out that the key feature responsible for the thermally activated low mobility is the band offset, which is related to the amount of charge transfer induced by the grain boundary trap states. There-

fore, reduction in the unoccupied trap state density at the grain boundary should lead to improvements in mobility, which could be possibly achieved through chemical tuning.[10,11,13] Direct investigation on the microscopic details of grain boundaries[35,36] could also be helpful in complementing the model understanding of transport at the grain boundary.

Increasing the grain size for Mg_3Sb_2-based compounds is clearly a successful strategy[17] but contrary to the usual strategy to decrease the grain size to scatter phonons.[37,38] In general, whether such strategy will be beneficial for thermoelectrics will depend on how much the lattice thermal conductivity reduction strategy relies on having small grains. Our model approach provides a quantitative basis for such optimizations of grain size using, for example, a quality factor analysis.[39]

It is worth noting that mitigation of the grain boundary influence is good for mobilites not only at low temperatures, but also at high temperatures where it no longer dominates the temperature dependence but still has measurable effects. These benefits can be gauged with our model as shown in Fig.5b which projects room for improvement in zT, in particular a $> 60\%$ improvement at room temperature. These estimates motivate the electronic aspect of grain boundary engineering in addition to the usual thermal[40,41] considerations.

4 Conclusions

We identify that, based on a variety of physical reasons, a Matthiessen's approach is not sufficient in describing transport in materials where strong influences of the grain boundary reduces the overall mobility of the material. A simple two-phase series circuit model accounting for the influence of grain boundaries as a separate phase is shown to successfully reproduce both the energy and temperature dependency of charge transport observed experimentally in $Mg_{3+x}Sb_{1.5}Bi_{0.5-y}Te_y$. Our model opens up opportunities for grain boundary engineering as a means for improving electronic materials.

Acknowledgements

Author contributions

JJK and SDK equally contributed to this project. JJK and SDK analyzed transport data, constructed the model, and wrote the manuscript. KI, HT, SO, and TK did the experiments that inspired the project and helped to validate the model. TK and GJS supervised the project. All authors edited the manuscript.

Conflict of interest

There are no conflicts to declare.

References

1 F. J. DiSalvo, *Science*, 1999, **285**, 703–706.

2 G. J. Snyder and A. H. Snyder, *Energy & Environmental Science*, 2017, **10**, 2280–2283.

3 H. Tamaki, H. K. Sato and T. Kanno, *Advanced Materials*, 2016, **28**, 10182–10187.

4 T.-R. Wei, G. Tan, X. Zhang, C.-F. Wu, J.-F. Li, V. P. Dravid, G. J. Snyder and M. G. Kanatzidis, *Journal of the American Chemical Society*, 2016, **138**, 8875–8882.

5 B. R. Ortiz, P. Gorai, L. Krishna, R. Mow, A. Lopez, R. McKinney, V. Stevanovic and E. S. Toberer, *Journal of Materials Chemistry A*, 2017, **5**, 4036–4046.

6 A. Zevalkink, W. G. Zeier, G. Pomrehn, E. Schechtel, W. Tremel and G. J. Snyder, *Energy & Environmental Science*, 2012, **5**, 9121.

7 R. He, D. Kraemer, J. Mao, L. Zeng, Q. Jie, Y. Lan, C. Li, J. Shuai, H. S. Kim, Y. Liu, D. Broido, C.-W. Chu, G. Chen and Z. Ren, *Proceedings of the National Academy of Sciences*, 2016, **113**, 13576–13581.

8 E. S. Toberer, A. Zevalkink, N. Crisosto and G. J. Snyder, *Advanced Functional Materials*, 2010, **20**, 4375–4380.

9 W. G. Zeier, A. Zevalkink, E. Schechtel, W. Tremel and G. J. Snyder, *Journal of Materials Chemistry*, 2012, **22**, 9826–9830.

10 S. Ohno, K. Imasato, S. Anand, H. Tamaki, S. D. Kang, P. Gorai, H. K. Sato, E. S. Toberer, T. Kanno and G. J. Snyder, *Joule*, 2018, **2**, 1–14.

11 J. Shuai, J. Mao, S. Song, Q. Zhu, J. Sun, Y. Wang, R. He, J. Zhou, G. Chen, D. J. Singh and Z. Ren, *Energy & Environmental Science*, 2017, **10**, 799–807.

12 J. Zhang, L. Song, S. H. Pedersen, H. Yin, L. T. Hung and B. B. Iversen, *Nature Communications*, 2017, **8**, 13901.

13 J. Mao, J. Shuai, S. Song, Y. Wu, R. Dally, J. Zhou, Z. Liu, J. Sun, Q. Zhang, C. dela Cruz, S. Wilson, Y. Pei, D. J. Singh, G. Chen, C.-W. Chu and Z. Ren, *Proceedings of the National Academy of Sciences*, 2017, **114**, 10548–10553.

14 J. Mao, Y. Wu, S. Song, J. Shuai, Z. Liu, Y. Pei and Z. Ren, *Materials Today Physics*, 2017, **3**, 1–6.

15 J. Mao, Y. Wu, S. Song, Q. Zhu, J. Shuai, Z. Liu, Y. Pei and Z. Ren, *ACS Energy Letters*, 2017, **2**, 2245–2250.

16 S. D. Kang and G. J. Snyder, *Nature Materials*, 2017, **16**, 252–257.

17 T. Kanno, H. Tamaki, H. K. Sato, S. D. Kang, J. Kuo, S. Ohno, K. Imasato, G. J. Snyder and Y. Miyazaki, *Applied Physics Letters*, 2018, **112**, 033903.

18 A. F. Mayadas and M. Shatzkes, *Physical Review B*, 1970, **1**, 1382–1389.

19 W. Steinhögl, G. Schindler, G. Steinlesberger and M. Engelhardt, *Physical Review B*, 2002, **66**, 075414.

20 A. Minnich, H. Lee, X. Wang, G. Joshi, M. Dresselhaus, Z. Ren, G. Chen and D. Vashaee, *Physical Review B*, 2009, **80**, 155327.

21 G. E. Pike and C. H. Seager, *Journal of Applied Physics*, 1979, **50**, 3414–3422.

22 H. F. Mataré, *Journal of Applied Physics*, 1984, **56**, 2605–2631.

23 J. de Boor, T. Dasgupta, H. Kolb, C. Compere, K. Kelm and E. Mueller, *Acta Materialia*, 2014, **77**, 68–75.

24 K. Imasato, S. D. Kang, S. Ohno and G. J. Snyder, *Materials Horizons*, 2018.

25 W. Taylor, N. Odell and H. Fan, *Physical Review*, 1952, **88**, 867.

26 J. Y. Seto, *Journal of Applied Physics*, 1975, **46**, 5247–5254.

27 S. D. Kang and G. J. Snyder, *ArXiv*, 2017, 1710.06896.

28 J. A. Hornbeck and J. R. Haynes, *Physical Review*, 1955, **97**, 311–321.

29 J. R. Haynes and J. A. Hornbeck, *Physical Review*, 1955, **100**, 606–615.

30 D. J. Bergman and O. Levy, *Journal of Applied Physics*, 1991, **70**, 6821–6833.

31 D. J. Bergman and L. G. Fel, *Journal of Applied Physics*, 1999, **85**, 8205–8216.

32 S. D. Kang, S. A. Danilkin, U. Aydemir, M. Avdeev, A. Studer and G. J. Snyder, *New Journal of Physics*, 2016, **18**, 013024.

33 M. S. Toprak, C. Stiewe, D. Platzek, S. Williams, L. Bertini, E. Müller, C. Gatti, Y. Zhang, M. Rowe and M. Muhammed, *Advanced Functional Materials*, 2004, **14**, 1189–1196.

34 H. X. Xin, X. Y. Qin, X. G. Zhu and Y. Liu, *Journal of Physics D: Applied Physics*, 2006, **39**, 375.

35 D. Y. Li, L. Guo, L. Li and H. Lu, *Scientific Reports*, 2017, **7**, 9673.

36 P. Puneet, R. Podila, M. Karakaya, S. Zhu, J. He, T. M. Tritt, M. S. Dresselhaus and A. M. Rao, *Scientific Reports*, 2013, **3**, 3212.

37 N. A. Heinz, T. Ikeda, Y. Pei and G. J. Snyder, *Advanced Functional Materials*, 2014, **24**, 2135–2153.

38 Y. Lan, A. J. Minnich, G. Chen and Z. Ren, *Advanced Functional Materials*, 2010, **20**, 357–376.

39 H. Wang, A. D. LaLonde, Y. Pei and G. J. Snyder, *Advanced Functional Materials*, 2013, **23**, 1586–1596.

40 H.-S. Kim, S. D. Kang, Y. Tang, R. Hanus and G. J. Snyder, *Materials Horizons*, 2016, **3**, 234–240.

41 K. Imasato, S. Ohno, S. D. Kang and G. J. Snyder, *APL Materials*, 2018, **6**, 016106.